Supplement Information

Dual-Mode Catalytic Degradation of Diclofenac by Copper Oxide-modified TiO_2/MnO_x Composites: Insights from Dark and UV-A Activation

Gloria Issa[‡], Sylvie Kříženecká[‡], Petr Bezdička[†], Daniela Popelková[†], Martin Kormunda[§], Jakub Ederer[‡], Daniel Bůžek[†,‡], Jan Čundrle[†,‡], Zdeněk Baďura[±,×], Jiří Henych[†,‡], Martin Šťastný[*†]

[‡]Institute of Organic Chemistry with Centre of Phytochemistry, Bulgarian Academy of Sciences, Ak. G. Bontchev str., bl.9, 1113, Sofia, Bulgaria

† Institute of Inorganic Chemistry of the Czech Academy of Sciences, 250 68 Husinec-Řež, Czechia

‡ Faculty of Environment, Jan Evangelista Purkyně University in Ústí nad Labem, Pasteurova 3632/15, 400 96 Ústí nad Labem, Czechia

§ Faculty of Science, Jan Evangelista Purkyně University in Ústí nad Labem, Pasteurova 3632/15, 400 96 Ústí nad Labem, Czechia

± Regional Centre of Advanced Technologies and Materials, Šlechtitelů 27, Olomouc 78371, Czech Republic

× Nanotechnology Centre, VŠB − Technical University of Ostrava, 17. listopadu 2172/15, 708 00 Ostrava-Poruba, Czech Republic

*Corresponding author's e-mail address: stastny@iic.cas.cz

Table of Contents

List of Tables

List of Figures

Figure S3. XPS spectra of Mn $2p_{3/2}$ for CuO-modified TiO_2, MnO_x, and their composites.

Figure S4. XPS spectra of Ti 2p for CuO-modified TiO_2, MnO_x, and their composites.

Figure S5. XPS spectra of O 1s for CuO-modified TiO_2, MnO_x, and their composites.

Figure S6. H_2 temperature-programmed reduction (H_2-TPR) profiles for CuO-modified TiO_2, MnO_x, and their composites.

Figure S7. Normalized degradation profile of DCF in control experiment under dark and UV conditions.

Figure S8. Stability and recyclability of the Cu/5Ti5Mn-HT catalyst over four consecutive DCF degradation cycles during dark and photocatalytic phases. (a) Normalized degradation profiles of DCF with inset showing the corresponding degradation efficiencies after 60 minutes. (b) Evolution of 5-hydroxy-diclofenac as the main transformation product across all cycles, indicating consistent degradation pathways and catalyst selectivity.

Figure S9. HPLC quantification of terephthalic acid (a) and 2-hydroxyterephthalic Acid (b) during dark and photocatalytic phases on Cu/2Ti8Mn-HT catalyst.

Figure S10. (+) ESI-MS spectrum of diclofenac (DCF) eluted at 6.69 min.

Figure S11. (+) ESI-MS spectrum of 5-hydroxy-diclofenac (5-OH-DCF) eluted at 5.90 min.

Figure S12. (+) ESI-MS spectrum of DP1 eluted at 6.73 min.

Figure S13. (+) ESI-MS spectrum of DP2 eluted at 5.35 min.

Figure S14. (+) ESI-MS spectrum of DP3 eluted at 4.01 min.

Figure S15. Time-dependent degradation of diclofenac and its products under dark and UV-A light conditions on Cu/2Ti8Mn-HT catalyst.

Figure S16. X-band CW-EPR spectrum of radical adducts trapped by PBN in an aqueous solution of Cu/5Ti5Mn-HT within a catalytic reaction at 113K (a) and 250K(b) after 15 minutes of continuous irradiation by UV light.

Figure S17. TOTH curves of CuO-modified TiO_2/MnO_x composite catalysts.

S1. Catalyst Preparation

Copper oxide-modified titania-manganese composites with Ti/Mn molar ratios of 2:8, 5:5, and 8:2, as well as copper oxide-modified TiO_2 and MnO_x, were synthesized using $TiCl_4$ and $MnCl_2{\cdot}4H_2O$ as precursors. Specifically, 12.0 g of N-hexadecyl-N, N, N-trimethylammonium bromide (CTAB) was dissolved in 100 mL of distilled water and mixed with 50 mL of an aqueous solution of the Ti and Mn precursors under stirring. The mixture was maintained at 50°C for 30 minutes, followed by the addition of 20 mL of a 25% ammonia solution drop-wise. After stirring overnight at 50°C, the product was cooled, decanted, filtered, and dried at room temperature.

Subsequently, the dried mixed catalysts were impregnated with copper using the IWI method with an aqueous $Cu(NO_3)_2{\cdot}3H_2O$ solution, followed by overnight drying at room temperature and calcination at 500°C for 4 hours. The overall copper content in all catalysts was 8 wt.%. The resulting catalyst samples were denoted as Cu/xTiyMn-HT, where x and y represent the molar ratios of Ti and Mn.

S2. Catalyst Characterization

The Brunauer–Emmett–Teller (BET) surface area, pore volume, and pore size distribution were obtained on a Quantachrome NOVA 1200e instrument, using nitrogen adsorption isotherms at 77 K. Solid samples were outgassed at 150 °C in vacuum before testing. The surface area

was calculated using the multipoint BET method based on adsorption data. The pore size distribution was determined using the Barrett–Joyner–Halenda (BJH) method using the desorption curve of the isotherm.

Diffraction patterns were collected with the PANalytical X´Pert PRO diffractometer equipped with a conventional X-ray tube (Cu K_α radiation, 40 kV, 30 mA) and a linear position sensitive detector PIXcel with an anti-scatter shield. A programmable divergence slit set to a fixed value of 0.5 deg., a Soller slit of 0.04 rad, and a mask of 15 mm were used in the primary beam. A programmable anti-scatter slit set to the fixed value of 0.5 deg., Soller slit of 0.04 rad, and Ni beta-filter were used in the diffracted beam. Data were collected in the range of 10 - 90 deg. 2theta with the step of 0.0131 deg. and 400s / step producing a scan of about 2 hours 51 minutes. The samples were mixed with an internal standard (50% of Si BDH) to estimate weight fractions of crystalline phases, including the amorphous content. This mixing was performed in an agate mortar in a powder suspension with acetone for about 15 minutes. Samples were then top-loaded into the conventional sample holders. Qualitative phase analysis was performed with the HighScorePlus software package (Malvern PANalytical, The Netherlands, version 5.2.0) [1], together with the PDF-5+ database [2]. The Profex 5.2.8 / BGMN 4.2.23 code was used to estimate weight fractions of crystalline phases, including the amorphous content and line profile analysis. This software performs the whole profile refinement using the Rietveld method [3–5]. All crystalline phase models were sourced from the PDF-5+ database [2].

An FEI Talos F200X (Thermo Fisher Scientific, NC, USA) transmission electron microscope was applied for the HRTEM analyses.

X-ray photoelectron spectroscopy (XPS) apparatus consisting of a SPECS PHOIBOS 100 hemispherical analyzer with a 5-channel detector and a SPECS XR50 achromatic X-ray source

equipped with an Al and Mg double anode was used to analyze the surface composition and chemical states of the elements in samples. The samples were placed on a sample holder with a well with a double side adhesive tape on bottom. A flood gun was not used. Collected spectra were processed using CasaXPS software (Version 2.3.25PR1.0), and raw spectra were pre-evaluated and calibrated in SpecsLab Prodigy (Version 4.29.2-r62520). Peak deconvolution was performed using a Shirley-type background, with Gaussian–Lorentzian GL(30) peak shapes and constrained full-width-at-half-maximum (FWHM) values. For the Mn $2p_{3}/_{2}$ region, spectra were deconvoluted into Mn^{2+}, Mn^{3+}, and Mn^{4+} components, following the assignment approach reported by Raja et al. [6]. The relative abundances of individual oxidation states were calculated from the integrated areas of the fitted peaks. Given the intrinsic spectral overlap and multiplet splitting of Mn 2p, these values are considered semi-quantitative and were used solely to compare relative oxidation state trends across the series.

The TPR/TG (temperature-programmed reduction/ thermogravimetric) analyses were performed in a Setaram TG92 instrument. in a flow of 50vol% H_2 in Ar (100 cm^3min^{-1}) and heating rate of 5 K min^{-1}.

FTIR spectra were recorded on a Bruker Vector 22 spectrometer at 1–2 cm^{-1} resolution, accumulating 64–128 scans and KBr pellets technique.

Raman investigation was carried out on a DXR Raman microscope (Thermo Fischer Scientific, Inc., Waltham, MA) equipped with a 532 nm laser.

Acid-base titrations were performed on an automatic titrator controlled by a PC (794 Basic Titrino, Metrohm, Switzerland) with a potentiometric endpoint determination. Typically, 250 mg of the sample catalyst was weighed into the titration vessel, and 50 mL of NaCl (0.1 mol/L), 3 mL of standardized solution of HCl (0.1 mol/L in 0.1 mol/L NaCl) and the suspension was mixed and bubbled by nitrogen for 30 minutes. Subsequently, the samples

were titrated with standardized 0.1 mol/L NaOH (in 0.1 mol/L NaCl) with continuous stirring with a magnetic bar under a nitrogen atmosphere. The rate of titrant was 0.1 mL/min in 0.05 mL aliquots.

EPR spectra were collected on X-band (~9.14–9.17 GHz) spectrometer JEOL JES-X-320 equipped by variable He temperature set-up ES-CT470 apparatus. The quality factor (Q) was kept above 6500 for all measurements to make the spectra comparable. As a sample holder, high-purity quartz tubes (Suprasil, Wilmad, ≤0.5 OD), and the accuracy of the g-values were determined by comparison with a Mn^{2+}/MgO standard (JEOL standard). The microwave power was set to 3.0 mW to avoid power saturation effects. A modulation width of 1-0.25 mT and a modulation frequency of 100 kHz were used. All EPR spectra were collected with a time constant of 30 ms and a sweep time of 2 min with four accumulations to improve the signal-to-noise ratio. In-situ light excitations EPR experiments (LEPR) were performed using a HeCd laser source operating @325 nm (max output power of 200 mW) from Kimmon Koha Co. Ltd (Tokyo, Japan). The UV light was shined directly onto the sample and kept frozen inside the cavity EPR resonator through its dedicated optical window.

S3. Analytical methods

Samples for routine DCF analysis, such as monitoring by-product evolution during catalytic/photocatalytic experiments, were analyzed by HPLC-DAD, and detection wavelength was 280 nm (absorption maximum of DCF and its main degradation product 5-hydroxy-diclofenac, 5-OH-DCF). Measurements were performed on a DIONEX UltiMate 3000 HPLC system equipped with a high-pressure pump, column thermostat, autosampler, and DAD detector. An Accucore PFP column (Thermo Scientific, USA) with dimensions of 150 x 4.6 mm and grain size of 2.6 µm was used to separate DCF and 5-OH-DCF. For gradient elution, the

mobile phase was acetonitrile and water, both acidified with formic acid (0.1%). **Table S1** presents the gradient elution settings. The mobile phase flow rate throughout the gradient was 1.0 mL/min. The separation occurred at 30 °C, and the column injection volume was 20 µL.

The intermediate by-products of DCF were meticulously analyzed using a liquid chromatography-tandem mass spectrometry (LC-MS/MS) system to elucidate the degradation pathways. Chromatographic separation was conducted on an Agilent 1290 Infinity II ultra-high-performance liquid chromatography (UHPLC) system (Agilent Technologies), employing an Accucore PFP analytical column (2.1 × 150 mm, 2.6 µm particle size). The flow rate was set at 0.4 mL/min, and the column temperature was maintained at 30 °C.

The mobile phase consisted of two components: (A) an aqueous solution of H_2O with 0.1% (v/v) formic acid and (B) acetonitrile, also containing 0.1% (v/v) formic acid. The gradient program commenced with 95% mobile phase A at 0 minutes, transitioning to 5% A from 9 to 11 minutes before returning to 95% A at 11.1 minutes. A post-run time of 3.9 minutes was included, ensuring the system returned to the initial gradient before the 15-minute stop time. Each sample was injected in a volume of 5 µL.

The HPLC system was coupled to an Agilent G6495A Triple Quadrupole mass spectrometer outfitted with an Agilent Jet Stream electrospray ionization source for effective ionization. Data acquisition was performed using Agilent MassHunter Acquisition software, while subsequent data analysis was carried out using Agilent MassHunter Workstation software. The mass spectrometric parameters for all analyzed compounds were optimized and are comprehensively summarized in **Table S2**.

The concentrations of TA and 2-OHTA in the reaction mixture were quantified using an Agilent 1260 Infinity II HPLC system equipped with a diode array detector (DAD). The analysis was

performed under the following conditions: a YMC Hydrosphere C18 column (50 mm x 4.6 mm, S-3 μm, 12 nm), a mobile phase consisting of 30% acetonitrile and 70% water, both acidified with 0.1% formic acid, a flow rate of 0.5 mL/min, a column temperature of 30°C, and an injection volume of 10 μL. The retention times were 2.1 minutes for TA and 4.44 minutes for 2-OHTA. Detection was carried out at 242 nm for TA and at 248 nm for 2-OHTA.

S4. Redox properties

Hydrogen temperature-programmed reduction (H_2-TPR) was used to analyze the reducibility of CuO-modified TiO_2/MnO_x catalysts. The deconvoluted TPR profiles (**Figure S6**) reveal distinct reduction behaviors for each catalyst, elucidating the interactions between Cu species and the TiO_2/MnO_x support. Multiple peaks in the reduction profiles indicate stepwise reduction processes involving different catalytic components. For the Cu/8Ti2Mn-HT catalyst, reduction peaks at 153°C and 225°C were observed. The 153°C peak corresponds to the reduction of surface CuO to metallic copper (Cu^0), suggesting a strong interaction between CuO and the TiO_2/MnO_x support [7]. The 225°C peak is attributed to the reduction of MnO_2 to Mn_2O_3, influenced by the TiO_2 matrix [8]. The Cu/5Ti5Mn-HT catalyst shows peaks at 179°C and 226°C. The 179°C peak represents CuO reduction to Cu^0, with a slightly higher temperature indicating a weaker interaction with the support compared to Cu/8Ti2Mn-HT. The 226°C peak is associated with MnO_2 reduction to Mn_2O_3. The Cu/2Ti8Mn-HT catalyst's peaks appear at 176°C and 234°C. The 176°C peak, indicating CuO reduction, is similar to Cu/5Ti5Mn-HT but shifted due to higher MnO_x content. The 234°C peak reflects MnO_2 reduction to Mn_2O_3, with the higher temperature suggesting stronger interactions between MnO_x species. The Cu/MnO_x-HT catalyst exhibits peaks at 275°C and 383°C. The 275°C peak

corresponds to CuO reduction to Cu^0, showing weaker interactions between CuO and MnO_x compared to TiO_2-containing samples. The 383°C peak is related to the reduction of bulk MnO_2 to Mn_2O_3 and Mn_3O_4 to MnO [9], highlighting higher MnO_x reducibility in the absence of TiO_2. The Cu/TiO_2-HT catalyst shows reduction peaks at 167°C and 203°C. The 167°C peak indicates CuO reduction to Cu^0, demonstrating strong CuO-TiO_2 interactions. The 203°C peak may correspond to the reduction of a secondary phase on TiO_2, reflecting the complexity of the reduction process.

S5. Fragmentation pathways and structural elucidation of degradation products

The mass spectral analysis of diclofenac, shown in **Figure S10**, revealed several key fragments. The fragment at m/z 137.2000, identified as a chlorine-substituted phenyl ring ($C_6H_4Cl^+$), results from the cleavage of the aromatic ring. Another prominent fragment at m/z 166.0000 corresponds to a dichlorinated phenyl ring ($C_6H_3Cl_2^+$). Additionally, the fragment at m/z 213.9000 represents a larger portion of diclofenac, including the aromatic ring and carboxylic acid group ($C_8H_6Cl_2NO^+$). The fragment at m/z 261.1000 indicates a structure combining aromatic rings with an amine group ($C_{14}H_{10}Cl_2NO^+$), while the peak at m/z 296.0000 corresponds to either the intact diclofenac molecule or a modified version ($C_{14}H_{10}Cl_2NO_2^+$). For 5-hydroxy-diclofenac (5-OH-DCF), the mass spectrum, depicted in **Figure S11**, shows fragments such as m/z 137.3000, a chlorine-substituted phenyl ring ($C_6H_4Cl^+$), and m/z 166.1000, a dichlorinated phenyl ring ($C_6H_3Cl_2^+$). The fragment at m/z 225.1000 corresponds to an aromatic ring with a hydroxylated carboxylic acid group ($C_8H_6Cl_2NO_2^+$), while the peak at m/z 313.5000 is attributed to the intact 5-OH-DCF molecule ($C_{14}H_{10}Cl_2NO_3^+$). The peak suggests further hydroxylation or additional modifications at m/z 332.6000 ($C_{14}H_{10}Cl_2NO_4^+$), and m/z 481.1000 indicates advanced fragmentation products or polymerization derivatives.

In the case of 2,6-dichloro-N-(o-tolyl)aniline (DP1), as shown in **Figure S12**, key fragments include m/z 137.1000 (chlorine-substituted phenyl ring, $C_6H_4Cl^+$), m/z 165.9000 (dichlorinated phenyl ring, $C_6H_3Cl_2^+$), and m/z 215.0000 (a larger portion including an aromatic ring with an amine group, $C_8H_6Cl_2N^+$). Significant peaks at m/z 253.1000 and m/z 296.0000 represent major fragments and the intact DP1 molecule ($C_{14}H_{11}Cl_2NO^+$). The peaks at m/z 333.1000 and m/z 391.2000 suggest further modifications or additional functional group attachments, while m/z 481.1000 indicates advanced fragmentation products.

The mass spectrum of 4-((2,6-dichlorophenyl)amino)-3-methylphenol (DP2), shown in **Figure S13**, reveals fragments such as m/z 137.2000 (chlorine-substituted phenyl ring, $C_6H_4Cl^+$), m/z 166.2000 (dichlorinated phenyl ring, $C_6H_3Cl_2^+$), and m/z 219.2000 (aromatic ring with a hydroxyl group and amine linkage, $C_8H_6Cl_2NO^+$). The peak at m/z 269.1000 corresponds to a major DP2 fragment ($C_{14}H_{11}Cl_2NO^+$), and m/z 286.0000 suggests the intact DP2 molecule ($C_{14}H_{11}Cl_2NO_2^+$). Further modifications are indicated by the peaks at m/z 333.1000 and m/z 435.1000, while m/z 481.1000 points to advanced fragmentation products involving multiple aromatic rings or extended conjugated systems.

Finally, the mass spectrum of 1-chloro-8-methyl-9H-carbazole (DP3), illustrated in **Figure S14**, shows fragments such as m/z 137.0000 (chlorine-substituted phenyl ring, $C_6H_4Cl^+$), m/z 168.2000 (dichlorinated phenyl ring, $C_6H_3Cl_2^+$), and m/z 217.1000 (carbazole structure with chlorine, $C_{12}H_8ClN^+$). The peak at m/z 250.0000 represents a major DP3 fragment ($C_{13}H_{10}ClN^+$), while m/z 296.0000 corresponds to the intact DP3 molecule ($C_{14}H_{11}ClN^+$). Additional modifications are suggested by peaks at m/z 333.1000 and m/z 481.1000.

S6. Evaluation of pH (PZC) and surface hydroxyl groups

Point of zero charge has been evaluated from titration curves, which have been transformed into curves corresponding to the total concentration of protons consumed in the titration process (TOTH) can be calculated from the following equation (TOTH. eq. S1):

$$TOTH = \frac{-(V_{NaOH} - V_{EP1}) \cdot c_{NaOH}}{V_0 + V_{HCl} + V_{NaOH}} (\frac{mol}{L}) \quad \text{(S1)}$$

where c_{NaOH} represents the concentration of NaOH. V_{NaOH} represents the volume of NaOH added at different titration points. V_{EP1} represents the volume of the first equivalent point. V_0 is the initial solution volume, and V_{HCl} represents the total volume of HCl added before titration [10]. The number of surface hydroxyl groups per solid weight (q) was calculated from the two equivalence points on the titration curve (V_{EP1} and V_{EP2}) by the following formula (eq. S2), and the results are presented in **Table S7** and **Figure S17**:

$$q = \frac{(V_{EP2} - V_{EP1}) \cdot c_{NaOH}}{m} \quad \text{(S2)}$$

Table S1. Gradient elution settings on the UltiMate 3000 liquid chromatograph for the determination of diclofenac (DCF) and its degradation intermediates.

Analyte	**Time [min]**	**%ACN 0.1% HCOOH**	**%Water 0.1% HCOOH**	**Flow rate (mL/min)**
Diclofenac (DCF) *5-hydroxy-diclofenac (5-OH-DCF)*	-2 min (equilibration)	35	65	1.0
	0 min	35	65	1.0
	4 min	95	5	1.0
	6 min	95	5	1.0

Table S2. Optimized mass spectrometric parameters for LC-MS/MS analysis.

Parameter	**Value**
Ionization mode	+ ESI with Agilent Jet Stream
Scan type	MS scan, 30 – 700 Da
Gas temperature	210 °C
Gas Flow	12 L/min
Nebulizer pressure	30 psi
Sheath gas temperature	400 °C
Sheath gas flow	12 L/min
Capillary voltage	3500 V
Nozzle voltage	0 V
Fragmentor	380 V

Table S3. Phase composition of CuO-modified titania–manganese catalysts.

Sample	Phase composition	Unit Cell Parameters, Å			Crystallite Size, nm
		a	b	c	
Cu/MnO_x-HT	Bixbyite (α-Mn_2O_3)	9.4123±0.0001	–	–	173.0±11.0
	Copper-Manganese Oxide ($Cu_{1.5}Mn_{1.5}O_4$)	8.2874±0.0004	–	–	22.0±0.4
	Manganese Oxide (Mn_5O_8)	10.3640±0.0009	5.7208±0.0006	4.8731±0.0006	25.5±1.1
Cu/TiO_2-HT	Anatase (TiO_2)	3.7865±0.0001	–	9.4994±0.0002	16.7±0.1
	Tenorite (CuO)	4.6798±0.0018	3.4341±0.0009	5.1256±0.0022	25.8±0.8
Cu/2Ti8Mn-HT	Bixbyite (α-Mn_2O_3)	9.4134±0.0011	–	–	40.0±6.4
	Copper-Manganese Oxide ($Cu_{1.5}Mn_{1.5}O_4$)	8.2871±0.0010	–	–	12.8±0.3
	Manganese Oxide (Mn_5O_8)	10.3882±0.0010	5.7416±0.0005	4.8764±0.0004	21.0±0.2
	Titanium Manganese oxide ($Ti_{0.9}Mn_{0.1}O_2$)	3.7922±0.0013	–	9.3059±0.0079	10.8±0.5
Cu/5Ti5Mn-HT	Bixbyite (α-Mn_2O_3)	9.4103±0.0034	–	–	848.8±0.0
	Copper-Manganese Oxide	8.2855±0.0012	–	–	35.4±3.0

	($Cu_{1.5}Mn_{1.5}O_4$)				
	Manganese Oxide (Mn_5O_8)	10.3866±0.0024	5.7383±0.0025	4.8825±0.0014	11.3±0.4
	Titanium Manganese oxide ($Ti_{0.9}Mn_{0.1}O_2$)	3.7879±0.0003	–	9.4316±0.0012	9.7±0.1
Cu/8Ti2Mn-HT	Bixbyite (α-Mn_2O_3)	9.4078±0.0028	–	–	35.7±6.0
	Copper-Manganese Oxide ($Cu_{1.5}Mn_{1.5}O_4$)	8.2860±0.0005	–	–	16.5±0.6
	Manganese Oxide (Mn_5O_8)	8.2860±0.0005	5.6757±0.0029	4.8350±0.0097	14.1±0.0
	Titanium Manganese oxide ($Ti_{0.9}Mn_{0.1}O_2$)	3.7860±0.0002	–	9.4546±0.0005	10.3±0.1

Table S4. Pseudo-first order kinetic model fitting parameters for diclofenac sodium (DCF) degradation by catalytic (in the dark) and photocatalytic decomposition (under UV-A irradiation) on CuO-modified TiO_2/MnO_x catalysts.

Sample	Degradation of diclofenac sodium (DCF)									
	Catalytic oxidation under dark (60 min)					Photocatalytic degradation under UV-A light (180 min)				
	k_{dark}±SE (min^{-1})[a]	$T_{1/2}$ (min)[b]	DCF_{cat} (%)[c]	$C_{5\text{-OH-DCF}}$ ($\mu g \cdot L^{-1} \cdot 60min^{-1}$)	r^2	k±SE (min^{-1})[a]	$T_{1/2}$ (min)[b]	r^2	TC (%)[d]	$C_{5\text{-OH-DCF}}$ ($\mu g \cdot L^{-1} \cdot 240min^{-1}$)
Cu/TiO_2-HT	0.0053 ±0.0001	130.8	12.0	38.8	0.963	0.007±0.0001	99.0	0.996	54.0	262.7
Cu/2Ti8Mn-HT	0.023 ±0.001	30.1	67.8	40.7	0.985	0.013±0.002	53.3	0.998	100	11.6
Cu/2Ti8Mn-HT-$AgNO_3$[†]	0.0082 ±0.0001	84.5	23.9	14.2	0.981	0.0048±0.0004	144.4	0.958	51.6	17.3
Cu/2Ti8Mn-HT-p-BQ[†]	0.021±0.001	33.0	67.1	38.4	0.961	0.0093±0.0004	74.5	0.994	93.7	12.4
Cu/2Ti8Mn-HT-IPA[†]	0.012±0.007	57.8	51.3	55.9	0.985	0.0008±0.0001	866.4	0.996	92.8	27.8

Cu/2Ti8Mn-HT-EDTA-2Na†	0.015±0.008	46.2	38.2	27.9	0.981	0.0098±0.0008	70.7	0.928	73.9	58.4
Cu/2Ti8Mn-HT-TA†	0.042±0.003	16.5	30.0	ND	0.999	0.0076±0.0004	91.2	0.999	68.9	ND
Cu/2Ti8Mn-HT_pH=4	0.028±0.002	24.8	78.8	48.7	0.988	0.0095±0.0005	73.0	0.999	100	8.7
Cu/2Ti8Mn-HT_pH=7	0.016±0.008	43.3	60.0	37.0	0.978	0.013±0.003	53.3	0.996	96.8	26.3
Cu/2Ti8Mn-HT_pH=9	0.0076±0.0003	91.2	27.8	14.2	0.996	0.0040±0.0002	173.3	0.965	50.0	17.3
Cu/5Ti5Mn-HT	0.079±0.001	8.8	99.8	144.7	0.995	ND	ND	ND	100	0
Cu/8Ti2Mn-HT	0.105±0.010	6.6	99.4	92.3	0.999	ND	ND	ND	100	0
Cu/MnO_x-HT	0.017±0.007	40.8	58.7	58.9	0.986	0.007±0.0003	99.0	0.986	87.9	73.4

[a] Reaction rate constants (*k, min^{-1}*) with standard errors (*SE*)

[b] Degradation half-time ($T_{1/2}$, *min*)

[c] DCF degraded in the dark (DCF_{cat}, *%)*

[d] 5-OH-DCF concentration after 60 or 240 min ($\mu g \cdot L^{-1}$)

[e] Total conversion (*TC*) of DCF at a time of 240 min (%)

† Reaction system with radical scavenger

Table S5. pH values of aqueous suspensions of individual catalysts.

Sample	**pH**
Cu/TiO_2-HT	5.65
Cu/MnO_x-HT	7.56
Cu/2Ti8Mn-HT	6.47
Cu/5Ti5Mn-HT	6.51
Cu/8Ti2Mn	6.41

Table S6. Degradation products identified in the DCF/Cu/2Ti8Mn-HT system.

Analyte/DP	**Retention time, t_R**	**Mass-to-charge**	**Formula**	**Proposed structure**

	(min)	**ratio (*m/z*)**		
DCF	6.69	295	$C_{14}H_{11}Cl_2NO_2$	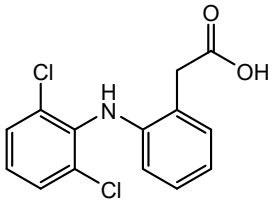
5-OH-DCF	5.90	312	$C_{14}H_{11}Cl_2NO_3$	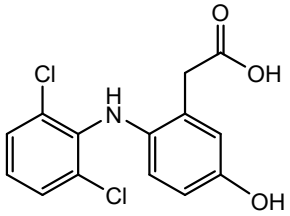
DP1	6.73	252	$C_{13}H_{11}Cl_2N$	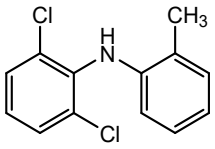
DP2	5.35	268	$C_{13}H_{11}Cl_2NO$	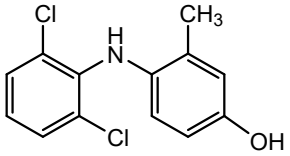
DP3	4.01	216	$C_{13}H_{10}ClN$	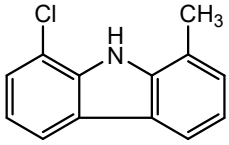

Table S7. The number of surface hydroxyl groups and pHPZC.

Sample	q_{-OH} (mmol/g)	pHPZC
Cu/MnO_x-HT	0.328	6.27
Cu/TiO_2-HT	0.291	4.75
Cu/5Ti5Mn-HT	0.917	4.21
Cu/8Ti2Mn-HT	0.899	7.52
Cu/2Ti8Mn-HT	0.326	4.84

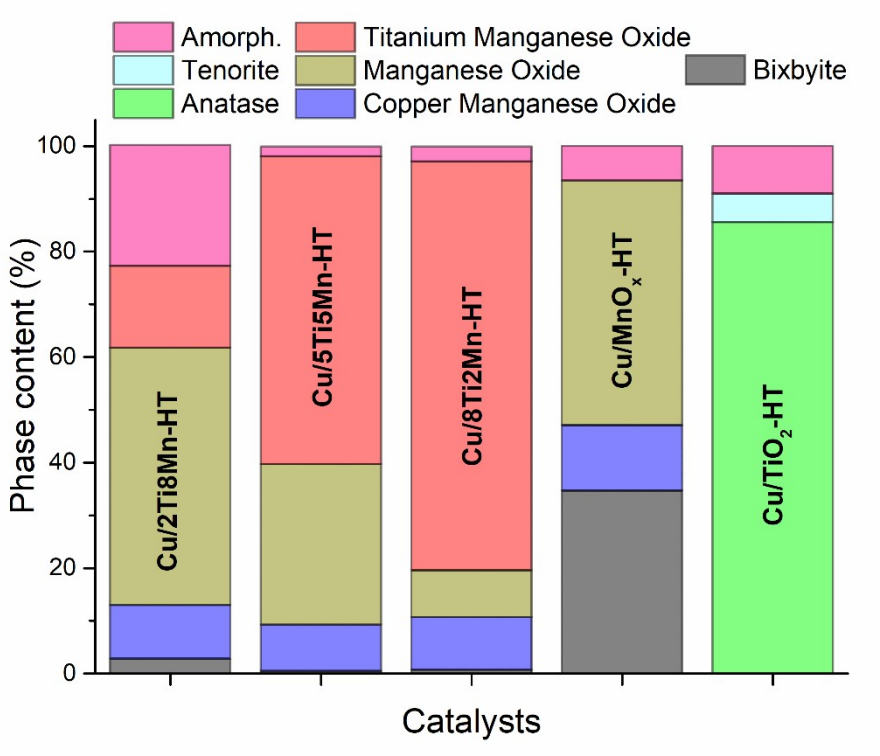

Figure S1. Phase ratio determined *via* QPA analysis for individual catalyst samples.

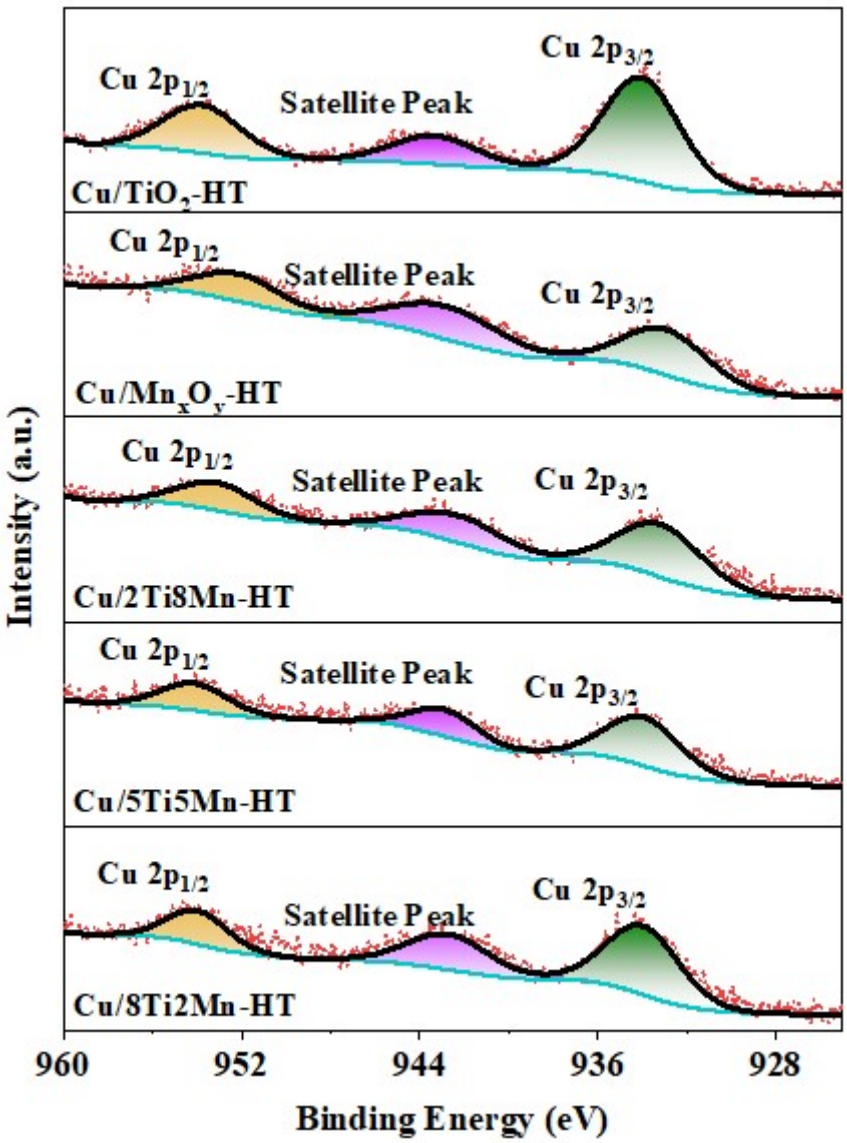

Figure S2. XPS spectra of Cu 2p for CuO-modified TiO_2, MnO_x, and their composites.

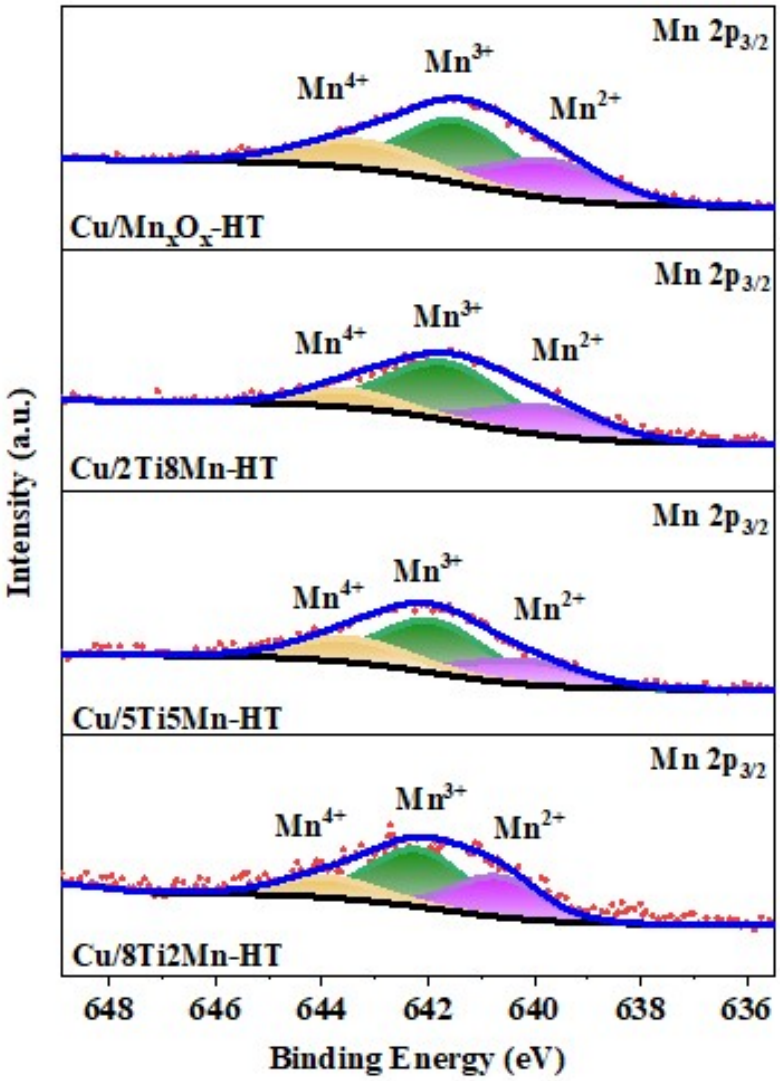

Figure S3. XPS spectra of Mn $2p_{3/2}$ for CuO-modified TiO_2, MnO_x, and their composites.

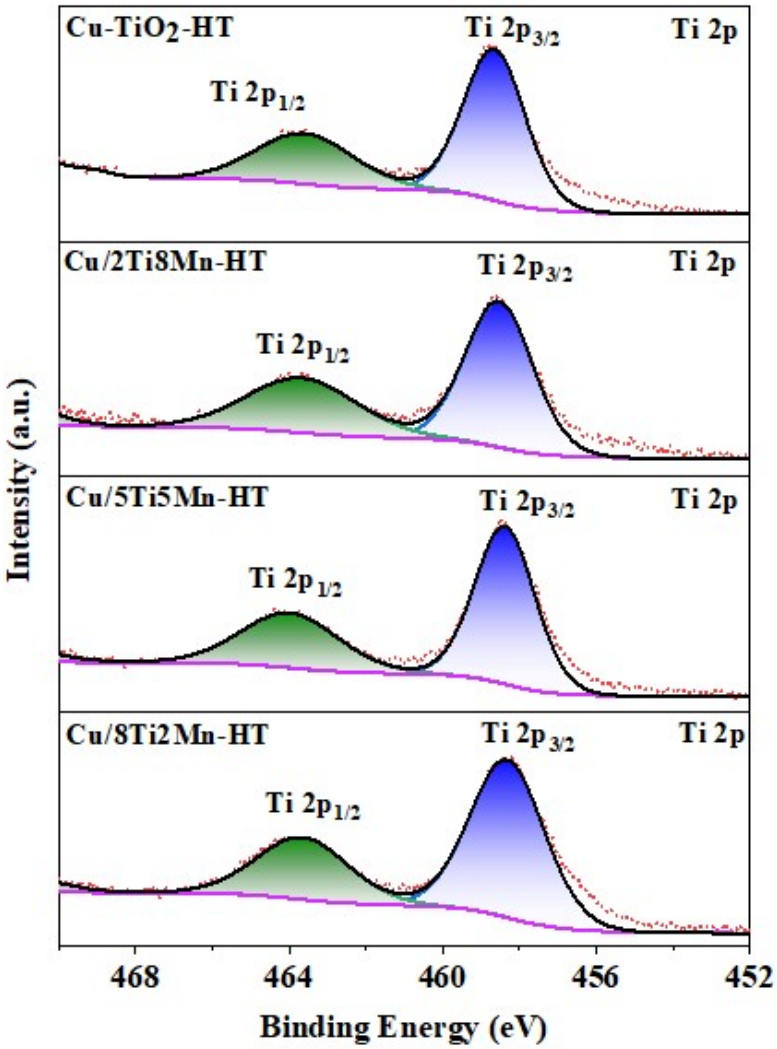

Figure S4. XPS spectra of Ti 2p for CuO-modified TiO_2, MnO_x, and their composites.

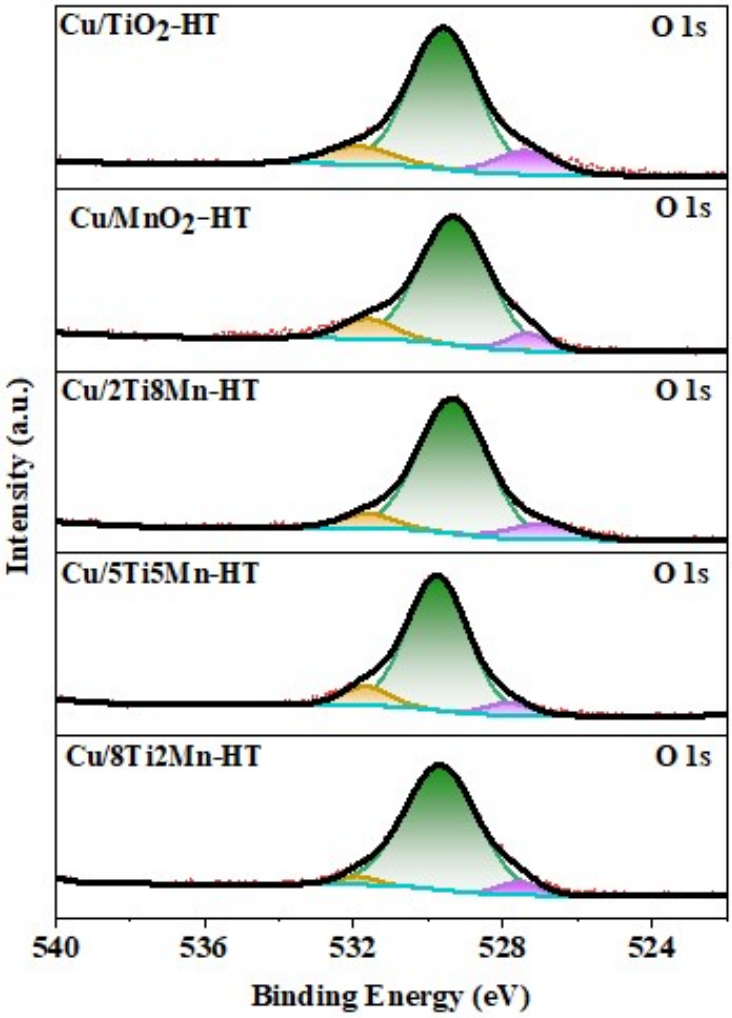

Figure S5. XPS spectra of O 1s for CuO-modified TiO_2, MnO_x, and their composites.

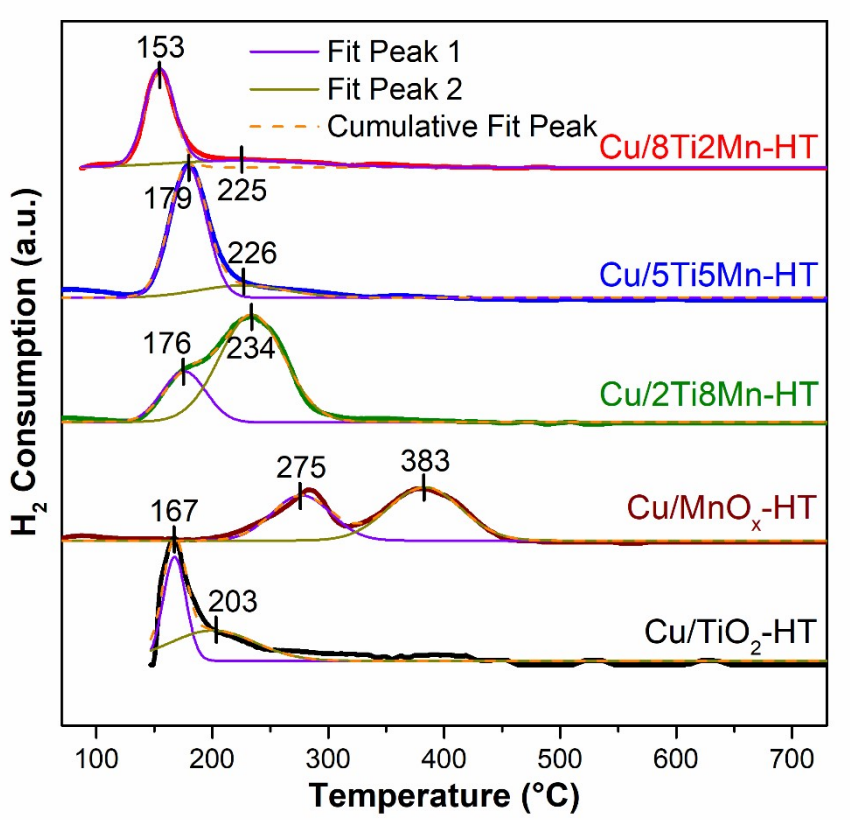

Figure S6. H_2 temperature-programmed reduction (H_2-TPR) profiles for CuO-modified TiO_2, MnO_x, and their composites.

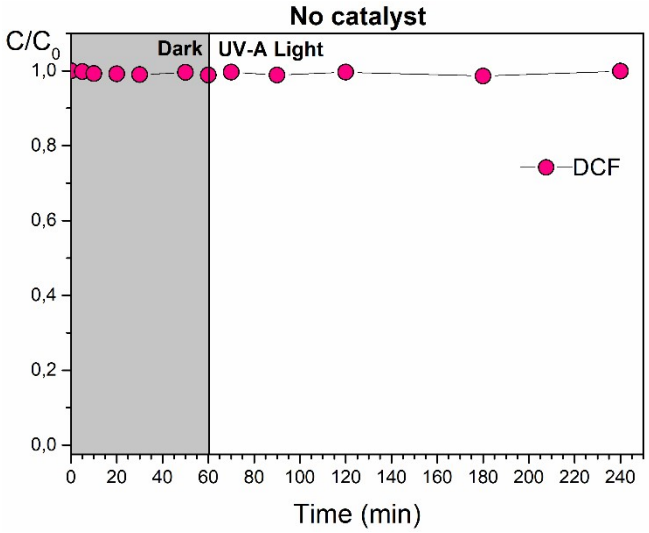

Figure S7. Normalized degradation profile of DCF in control experiment under dark and UV conditions.

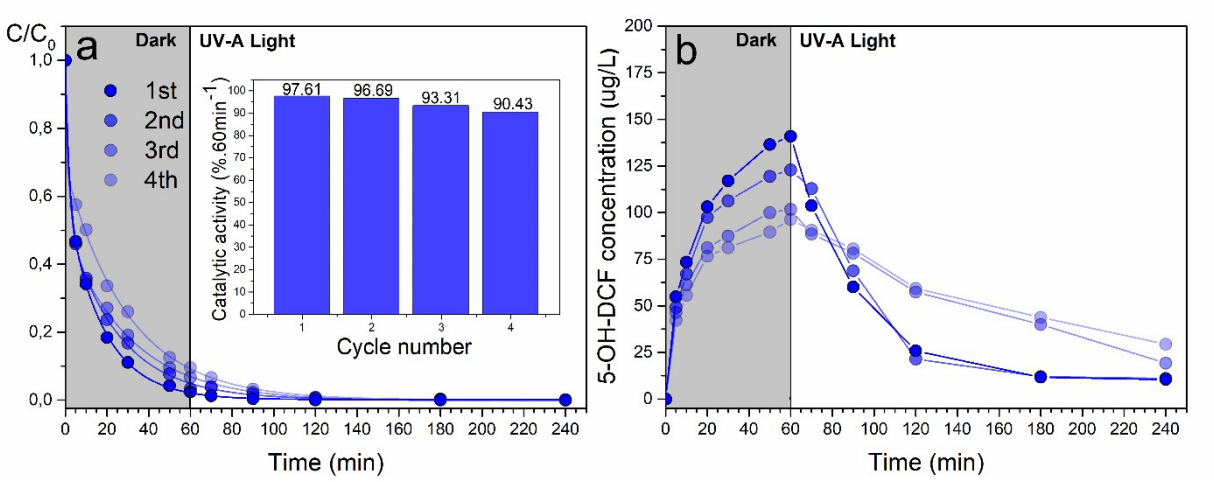

Figure S8. Stability and recyclability of the Cu/5Ti5Mn-HT catalyst over four consecutive DCF degradation cycles during dark and photocatalytic phases. (a) Normalized degradation profiles of DCF with inset showing the corresponding degradation efficiencies after 60 minutes. (b) Evolution of 5-hydroxy-diclofenac as the main transformation product across all cycles, indicating consistent degradation pathways and catalyst selectivity.

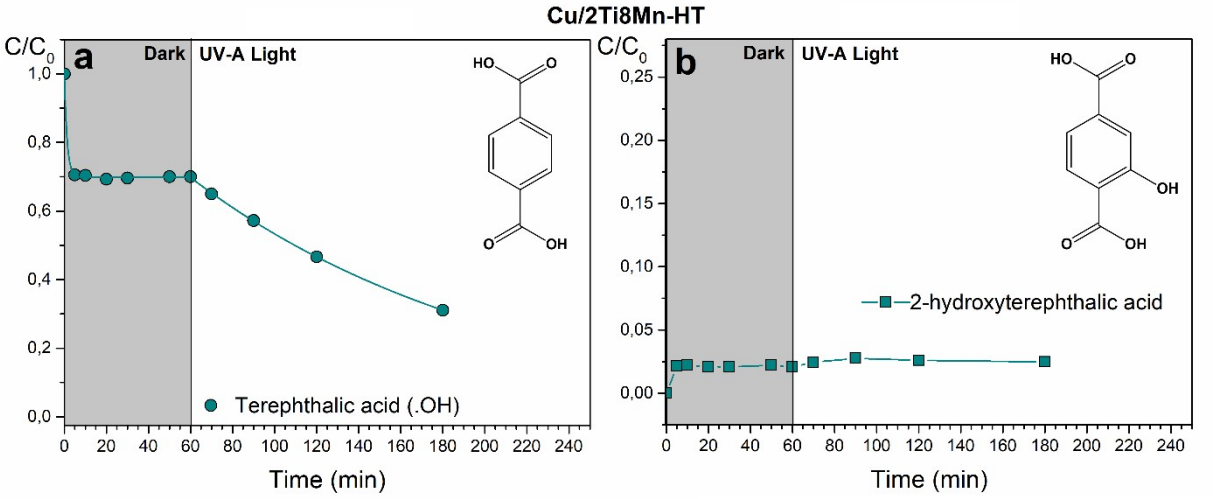

Figure S9. HPLC quantification of terephthalic acid (a) and 2-hydroxyterephthalic Acid (b) during dark and photocatalytic phases on Cu/2Ti8Mn-HT catalyst.

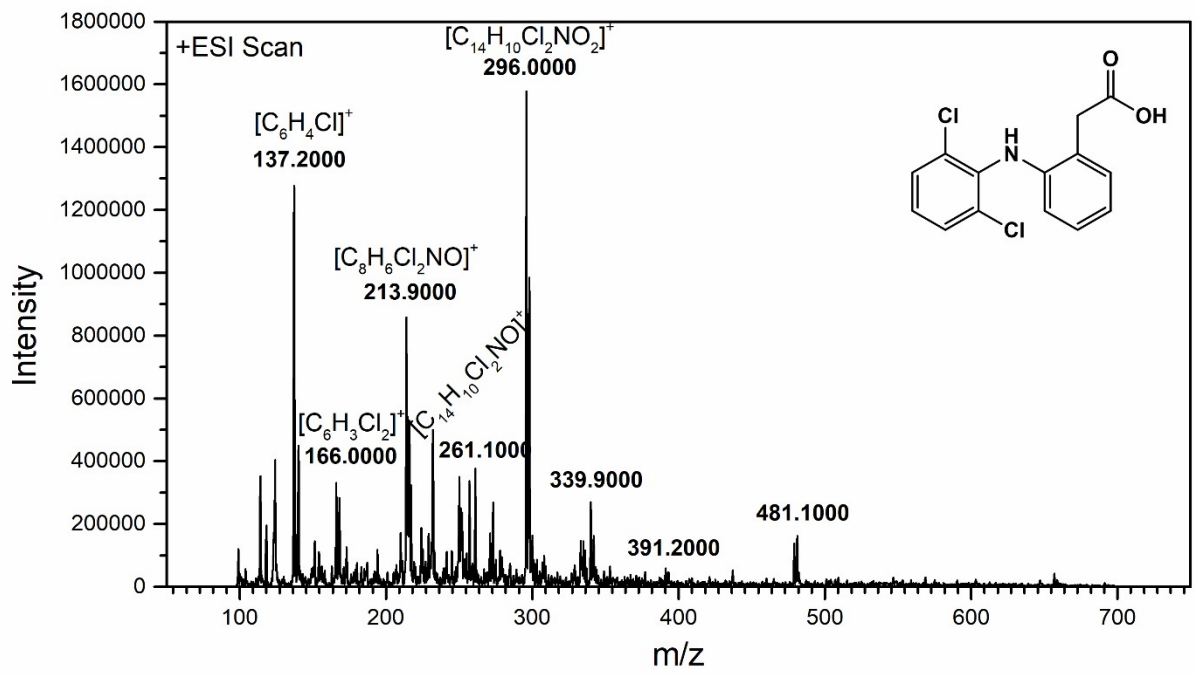

Figure S10. (+) ESI-MS spectrum of diclofenac (DCF) eluted at 6.69 min.

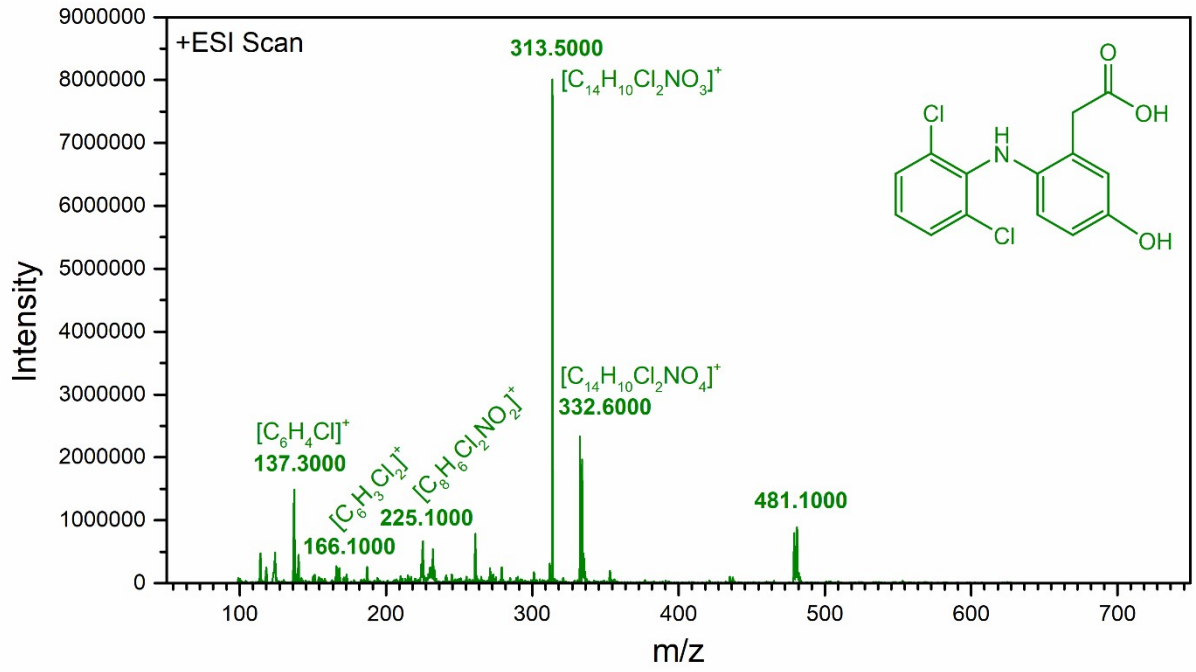

Figure S11. (+) ESI-MS spectrum of 5-hydroxy-diclofenac (5-OH-DCF) eluted at 5.90 min.

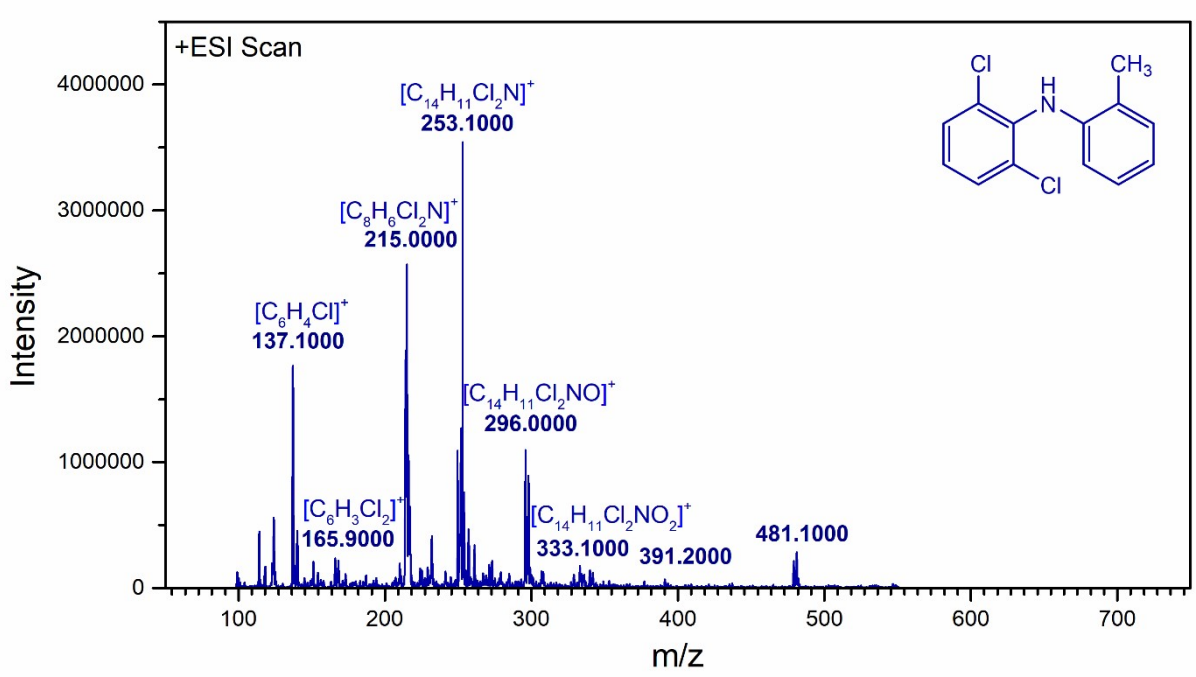

Figure S12. (+) ESI-MS spectrum of DP1 eluted at 6.73 min.

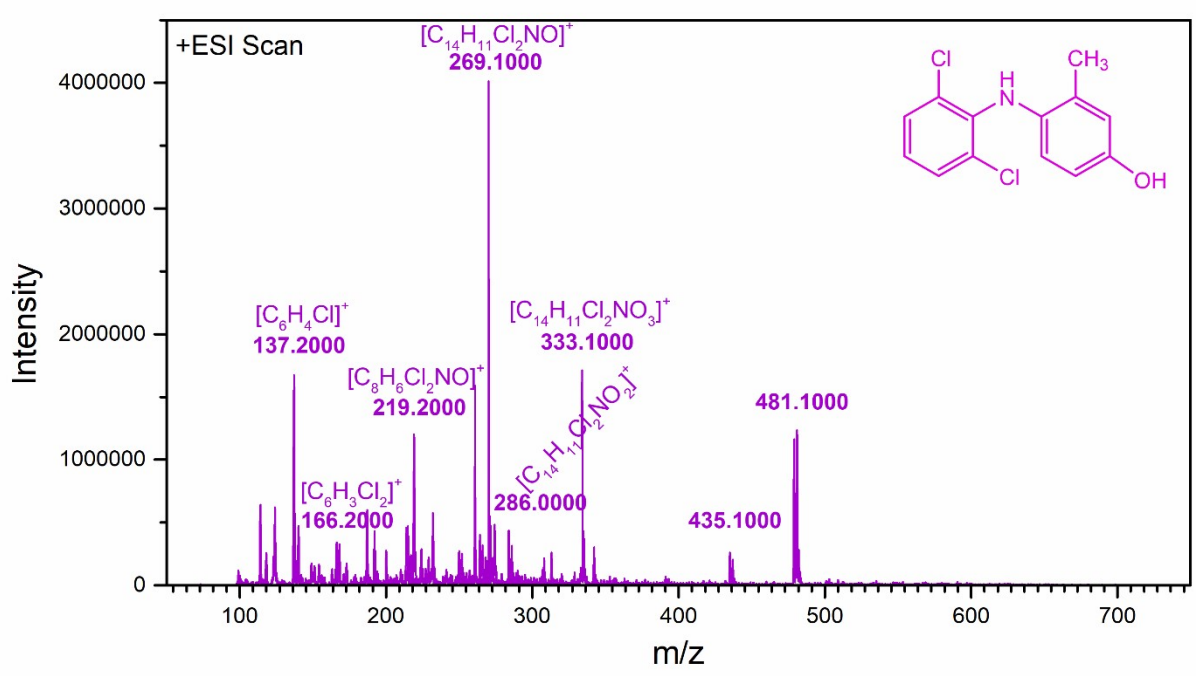

Figure S13. (+) ESI-MS spectrum of DP2 eluted at 5.35 min.

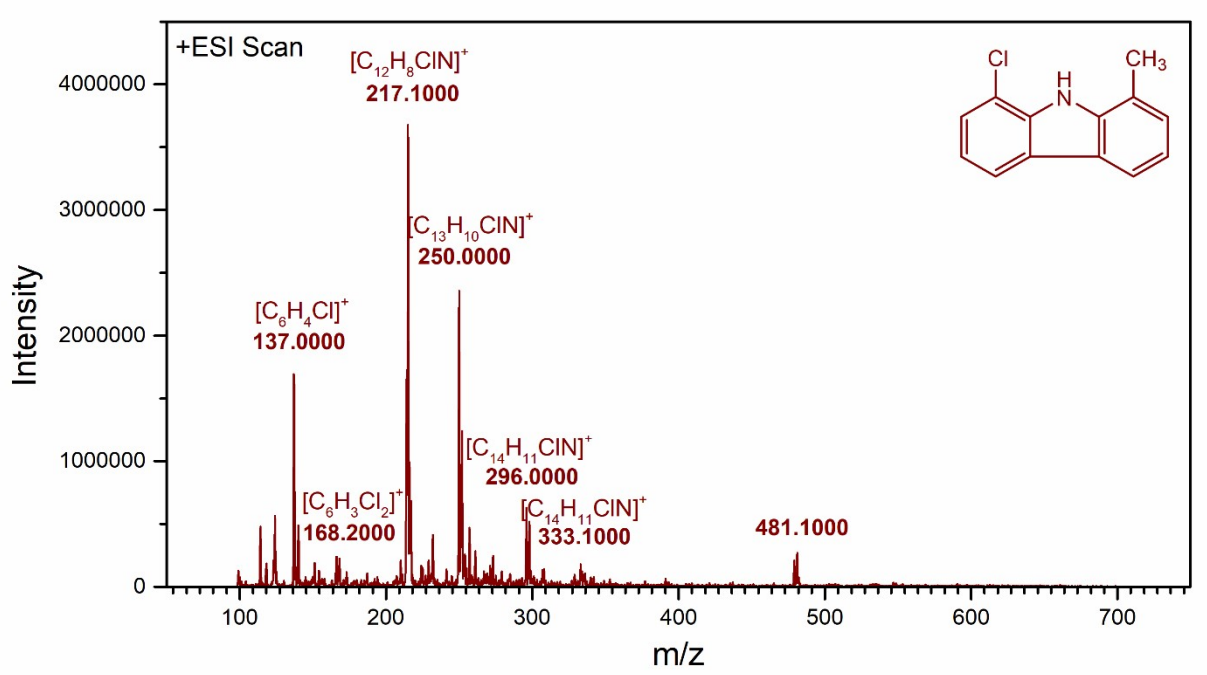

Figure S14. (+) ESI-MS spectrum of DP3 eluted at 4.01 min.

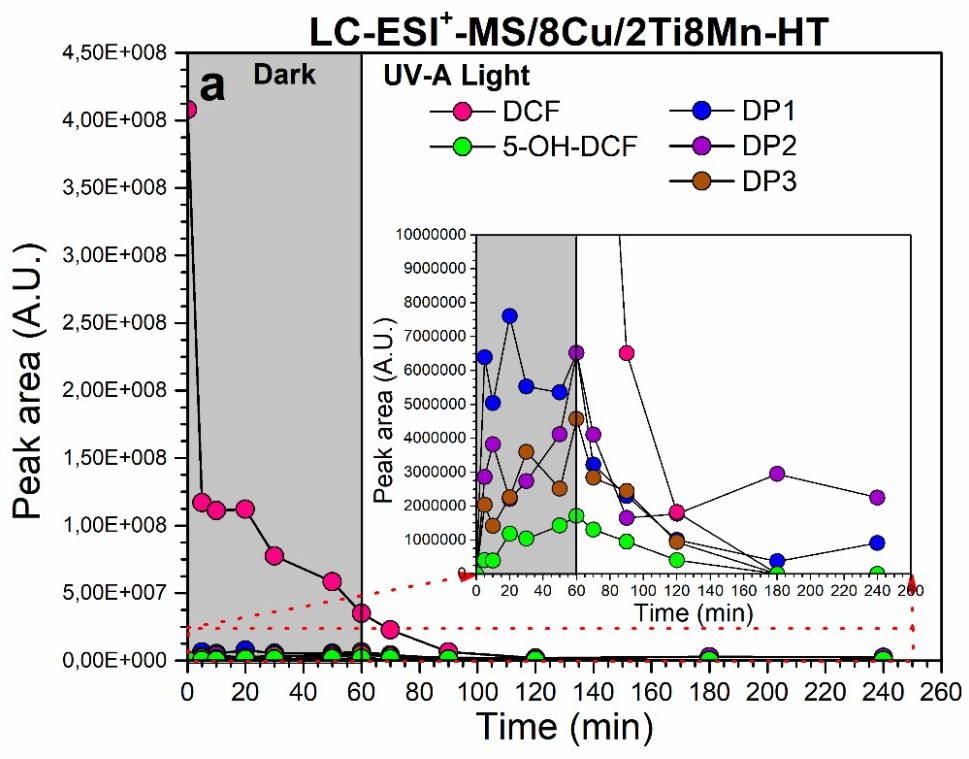

Figure S15. Time-dependent degradation of diclofenac and its products under dark and UV-A light conditions on Cu/2Ti8Mn-HT catalyst.

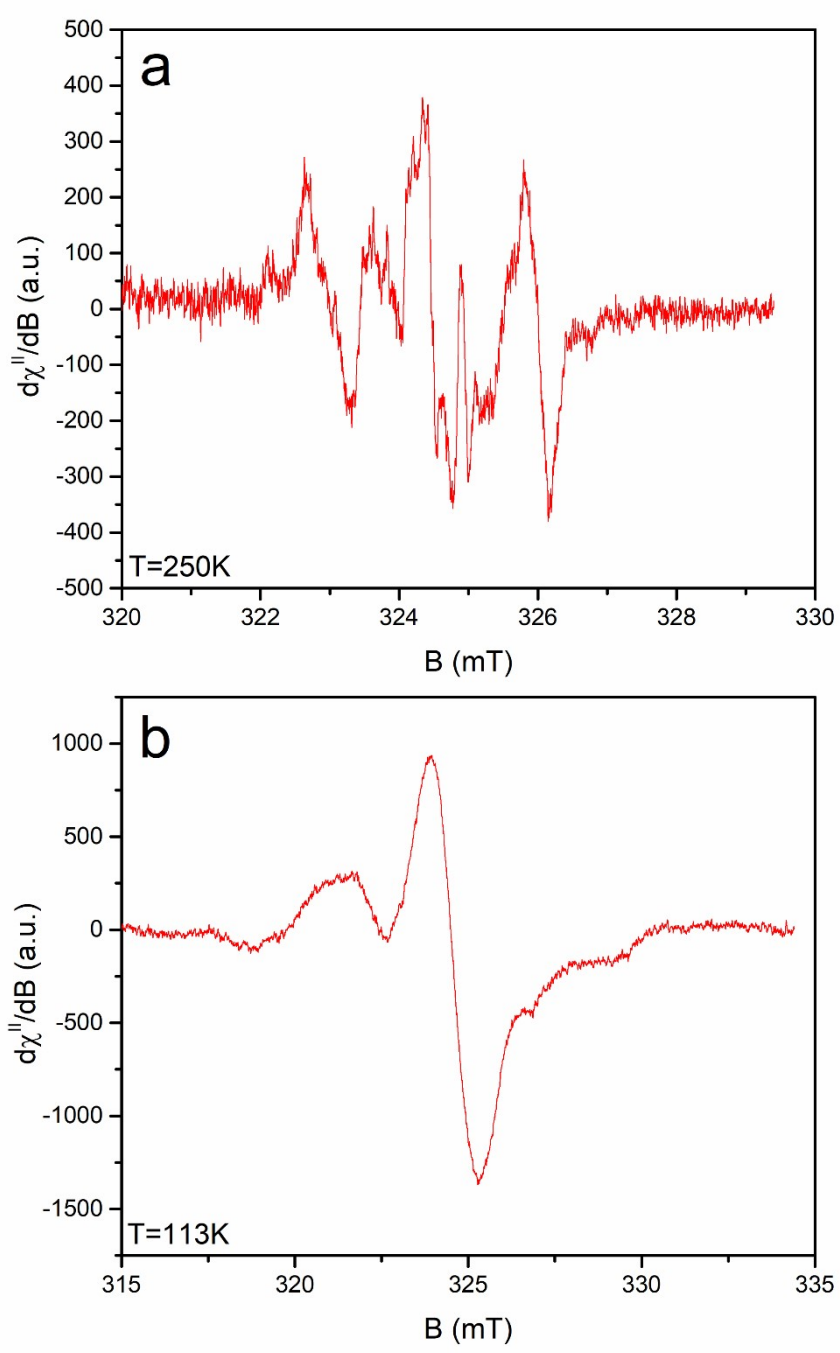

Figure S16. X-band CW-EPR spectrum of radical adducts trapped by PBN in an aqueous solution of Cu/5Ti5Mn-HT within a catalytic reaction at 113K (a) and 250K(b) after 15 minutes of continuous irradiation by UV light.

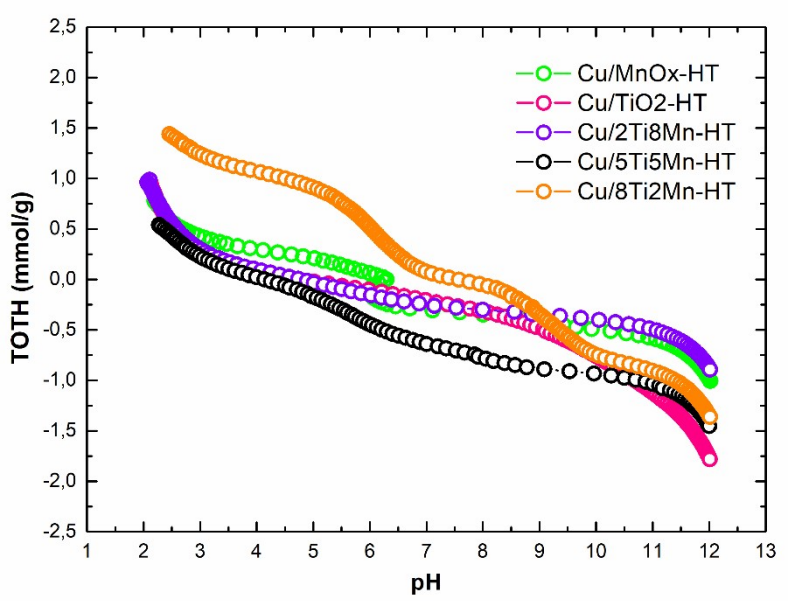

Figure S17. TOTH curves of CuO-modified TiO_2/MnO_x composite catalysts.

References

[1] T. Degen, M. Sadki, E. Bron, U. König, G. Nénert, The HighScore suite, Powder Diffr. 29 (2014) S13–S18. https://doi.org/10.1017/S0885715614000840.

[2] S.N. Kabekkodu, A. Dosen, T.N. Blanton, PDF-5+: a comprehensive powder diffraction file™ for materials characterization, Powder Diffr. (2024) 1–13. https://doi.org/10.1017/S0885715624000150.

[3] J. Bergmann, P. Friedel, R. Kleeberg, BGMN—a new fundamental parameters based Rietveld program for laboratory X-ray sources, its use in quantitative analysis and structure investigations, CPD Newsl. 20 (1998) 5–8.

[4] J. Bergmann, T. Monecke, R. Kleeberg, Alternative algorithm for the correction of preferred orientation in Rietveld analysis, J. Appl. Crystallogr. 34 (2001) 16–19. https://doi.org/10.1107/S002188980001623X.

[5] N. Doebelin, R. Kleeberg, Profex: a graphical user interface for the Rietveld refinement

program BGMN, J. Appl. Crystallogr. 48 (2015) 1573–1580. https://doi.org/10.1107/S1600576715014685.

[6] S. Raja, M.S. Alphin, L. Sivachandiran, P. Singh, D. Damma, P.G. Smirniotis, TiO2-carbon nanotubes composite supported MnOx-CuO catalyst for low-temperature NH3-SCR of NO: Investigation of SO2 and H2O tolerance, Fuel. 307 (2022) 121886. https://doi.org/10.1016/j.fuel.2021.121886.

[7] S. Zeng, W. Zhang, M. Śliwa, H. Su, Comparative study of CeO2/CuO and CuO/CeO2 catalysts on catalytic performance for preferential CO oxidation, Int. J. Hydrogen Energy. 38 (2013) 3597–3605. https://doi.org/10.1016/j.ijhydene.2013.01.030.

[8] Z. Liu, J. Zhu, J. Li, L. Ma, S.I. Woo, Novel Mn–Ce–Ti Mixed-Oxide Catalyst for the Selective Catalytic Reduction of NO x with NH 3, ACS Appl. Mater. Interfaces. 6 (2014) 14500–14508. https://doi.org/10.1021/am5038164.

[9] J. Wang, H. Zhao, J. Song, T. Zhu, W. Xu, Structure-Activity Relationship of Manganese Oxide Catalysts for the Catalytic Oxidation of (chloro)-VOCs, Catalysts. 9 (2019) 726. https://doi.org/10.3390/catal9090726.

[10] X. Ren, J. Li, X. Tan, X. Wang, Comparative study of graphene oxide, activated carbon and carbon nanotubes as adsorbents for copper decontamination., Dalton Trans. 42 (2013) 5266–5274. https://doi.org/10.1039/c3dt32969k.